Available online at www.sciencedirect.com
SCIENCE DIRECT®
Physica E 18 (2003) 372–382
PHYSICA E
www.elsevier.com/locate/physe

Electron scattering on disordered double-barrier GaAs–$Al_xGa_{1-x}As$ heterostructures

I. Gómez[a,*], E. Diez[a], F. Domínguez-Adame[a], P. Orellana[b]

[a] *GISC, Departamento de Física de Materiales, Universidad Complutense, E-20840 Madrid, Spain*
[b] *Departamento de Física, Universidad Católica del Norte, Casilla 1280, Antofagasta, Chile*

Received 26 August 2002; received in revised form 30 October 2002; accepted 15 November 2002

Abstract

We present a novel model to calculate vertical transport properties such as conductance and current in unintentionally disordered double-barrier GaAs–$Al_xGa_{1-x}As$ heterostructures. The source of disorder comes from interface roughness at the heterojunctions (lateral disorder) as well as spatial inhomogeneities of the Al mole fraction in the barriers (compositional disorder). Both lateral and compositional disorder break translational symmetry along the lateral direction and therefore electrons can be scattered off the growth direction. The model correctly describes channel mixing due to these elastic scattering events. In particular, for realistic degree of disorder, we have found that the effects of compositional disorder on transport properties are negligible as compared to the effects due to lateral disorder.

PACS: 73.20.Dx; 72.10. − d; 72.10.Fk

Keywords: Disorder; Electronic transport; Conductance; Double barrier

1. Introduction

Resonant tunneling (RT) through double-barrier structures (DBS) make these systems very promising candidates for a new generation of ultra-high speed electronic devices. For instance, a GaAs–$Ga_{1-x}Al_xAs$ DBS operating at THz frequencies has been reported in the literature [1]. The basic reason for RT to arise in DBS is a quantum phenomenon whose fundamental characteristics are by now well understood: There exists a dramatic increase of the electron transmission whenever the energy of the incident electron is close to one of the unoccupied quasi-bound-states inside the well [2]. In practice, a bias voltage is applied to shift the energy of this quasi-bound-state of nonzero width so that its center matches the Fermi level. Consequently, the j–V characteristics present negative differential resistance when the quasi-bound-state lies well below the Fermi level.

In actual samples, however, the situation is much more complex than this simple picture. Scattering by phonons, electrons or defects reduces the required quantum coherence and, in fact, deviations from the above simple description are observed. These scattering mechanisms explain the occurrence of side-band resonant peaks due to the interaction with phonons [3,4] and photons [5,6], hysteresis in the j–V characteristics due to many body effects [7–9], and the

* Corresponding author. Tel.: +34-91-394-50-12; fax: +34-91-394-45-47.
E-mail address: igcuesta@valbuena.fis.ucm.es (I. Gómez).

1386-9477/03/$ - see front matter
doi:10.1016/S1386-9477(02)01120-7

decrease of electron mobility due to rough surfaces even in good-quality heterostructures [10]. While one-dimensional models successfully describe scattering by electrons and phonons, they obviously cannot account for all interface roughness effects. So far, there are analytical results concerning the propagation of wave packets in a randomly layered medium when the potential is a random function of only one coordinate [11], but for a small number of layers, as in DBS, in-plane disorder becomes important and one expects such approaches to fail. Realistic models of in-plane disorder, including power-like or exponential spatial correlations observed by scanning tunneling microscopy, usually lead to intractable analytical models; hence the importance of numerically solvable models to bridge this gap. An important contribution was already provided by Henrickson et al., who applied the tight-binding Green function method to interface roughness in DBS [12]. In this paper transmission was studied for a DBS with a rather simple model of disorder (periodic roughness with random relative phases at the interfaces). A level splitting was found for narrow well DBS and a dependence on the roughness lateral size was observed.

In this work we present a two-dimensional model of vertical transport in semiconductor heterostructures that allowed us to carry out an extensive study of electron scattering by interface roughness. In particular, we aim to elucidate the relationship between macroscopic properties of the DBS (e.g. conductance) with microscopic parameters of the model (e.g. correlation length of the surface disorder). The paper is organized as follows. The body of the paper is Section 2, where we present our model based on the effective-mass approximation, describing a disordered sample (e.g. an imperfect DBS) connected to two perfectly ohmic leads (see Fig. 1). The Ben Daniel–Duke equation is discretized, boundary conditions are discussed and scattering solutions are found by means of the transfer-matrix method for *any* arbitrary heterostructure made of wide-gap semiconductors. Afterwards, expressions for two-terminal conductance and current for unintentionally disordered DBS are provided. The model is worked out in a two-dimensional space for computational limitations, although it will be clear that generalization to three dimensions is rather straightforward. Section 3 describes the various models of disorder we have used to mimic structural

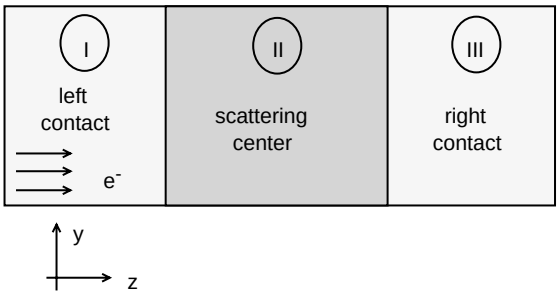

Fig. 1. Schematic view of the sample. Regions I and III are the electrical leads of the sample (contacts) and electrons undergo scattering processes only at region II.

data obtained by transmission electron microscopy and X-ray scattering. In Section 4 we present the numerical results and, in particular, the relationship between macroscopic properties of the DBS with microscopic parameters of the model. Finally, in Section 5 we discuss our results and the main conclusions of the work.

2. Model

2.1. Discrete equation

We consider the single-electron two-dimensional Schrödinger equation within the framework of the one-band effective-mass approximation. Close to the Γ valley, this approach leads to the Ben Daniel–Duke equation for the envelope function

$$\left[-\frac{\hbar^2}{2m^*}\left(\frac{\partial^2}{\partial y^2}+\frac{\partial^2}{\partial z^2}\right)+U(y,z)\right]\psi(y,z) = E\psi(y,z), \tag{1}$$

where z denotes the coordinate along the growth direction (see Fig. 1). Notice that we have taken a constant effective mass m^* at the Γ valley although this is not a serious limitation as the model can be easily generalized to include a position-dependent effective mass. We then consider a mesh with lattice spacings a_y and a_z in the y and z directions, respectively. Defining $t_y \equiv -\hbar^2/(2m^*a_y^2)$ and $t_z \equiv -\hbar^2/(2m^*a_z^2)$, we arrive at the following discretized version of Eq. (1),

$$t_z(\psi_{n+1,m}+\psi_{n-1,m})+t_y(\psi_{n,m+1}+\psi_{n,m-1}) + (U_{n,m}-2t_z-2t_y)\psi_{n,m} = E\psi_{n,m}. \tag{2}$$

The potential term $U_{n,m}$ in Eq. (2) is given by the conduction-band edge energy at the point (na_y, ma_z) which, in turn, depends on the Al mole fraction in the vicinity of that position. Consequently, both kinds of disorder (lateral and compositional) are taken into account through this diagonal term (diagonal disorder).

2.2. Transfer matrix formalism

In order to solve the tight-binding-like Eq. (2) we use the transfer matrix method based on the solutions calculated for each slide of the system (a portion of the system with index n constant) along the z direction. To this end, we define

$$\phi_n \equiv \begin{pmatrix} \psi_{n,1} \\ \psi_{n,2} \\ \vdots \\ \psi_{n,M} \end{pmatrix}, \quad n = 0, 1, \ldots, N+1 \tag{3}$$

and

$$\mathscr{M}_n = \begin{pmatrix} U_{n,1} - 2t_z - 2t_y & t_y & 0 & \cdots & t_y \\ t_y & U_{n,2} - 2t_z - 2t_y & t_y & \cdots & 0 \\ 0 & t_y & U_{n,3} - 2t_z - 2t_y & \cdots & 0 \\ \vdots & \vdots & \vdots & \ddots & \vdots \\ t_y & 0 & 0 & \cdots & U_{n,M} - 2t_z - 2t_y \end{pmatrix}. \tag{4}$$

Here M and $N+1$ are the number of mesh divisions in the y and z directions, respectively. Note that periodic boundary conditions have been taken into account on each slide, $(\mathscr{M}_n)_{1M} = (\mathscr{M}_n)_{M1} = t_y$. With these definitions, Eq. (2) can be cast in a more compact form

$$\begin{pmatrix} \phi_{n-1} \\ \phi_n \end{pmatrix} = \begin{pmatrix} t_z^{-1}(E\mathscr{I} - \mathscr{M}_n) & -\mathscr{I} \\ \mathscr{I} & \mathscr{O} \end{pmatrix} \times \begin{pmatrix} \phi_n \\ \phi_{n+1} \end{pmatrix}, \tag{5}$$

where $\mathscr{I}$ and $\mathscr{O}$ are the $M \times M$ identity and null matrices, respectively. This expression allows us to relate by iteration the envelope-function amplitudes at non-consecutive slides. In particular, we can obtain the expression of the envelope-function amplitudes in the left contact as a function of the amplitudes in the right one

$$\begin{pmatrix} \phi_0 \\ \phi_1 \end{pmatrix} = \mathscr{T}^{(N)} \begin{pmatrix} \phi_N \\ \phi_{N+1} \end{pmatrix}, \tag{6}$$

where

$$\mathscr{T}^{(N)} \equiv \prod_{n=1}^{N} \begin{pmatrix} t_z^{-1}(E\mathscr{I} - \mathscr{M}_n) & -\mathscr{I} \\ \mathscr{I} & \mathscr{O} \end{pmatrix} \tag{7}$$

is the transfer matrix for the heterostructure.

2.3. Scattering solutions

We are interested in the scattering of electrons incident from the left contact. The envelope functions within the contacts will be determined by the boundary conditions. These boundary conditions are open in the z direction, and periodic on each slide, that is in the y direction. The former implies plane wave solutions in the z-axis, and the latter yield an energy discretization on y. As a consequence, this discretization results in a number of transverse channels equal to the number of points in the transverse mesh direction. Considering by the moment $U_{n,m} = 0$ at the contacts and setting $\psi_{n,1} = \psi_{n,M+1}$, a particular solution of Eq. (2) is given by

$$\psi^l_{n,m} = \frac{1}{\sqrt{\mathscr{N}_l}} \mathrm{e}^{\mathrm{i}\frac{2\pi l}{M}m} \mathrm{e}^{\mathrm{i}k_l a_z n}, \quad l = 1, 2, \ldots, M. \tag{8}$$

Here $\mathscr{N}_l$ is a normalization constant that is needed for the different *propagating* modes to carry the same current all of them. This normalization constant is given by

$$\mathscr{N}_l = \frac{1}{a_y^2} \sin^2\left(\frac{2\pi l}{M}\right) + \frac{1}{a_z^2} \sin^2(k_l a_z). \tag{9}$$

Note that we consider a dependence on the index l of the momentum in the z direction. This is a consequence of the implicit assumption that all the scattering processes in region II (see Fig. 1) are elastic, so energy is conserved. Thus, for a given energy,

$$k_l = \frac{1}{a_z}\cos^{-1}\left\{\frac{1}{2t_z}\left[E - 2t_y\left(\cos\frac{2\pi l}{M} - 1\right)\right] + 1\right\}. \tag{10}$$

Finally, we can write a general solution of the scattering problem for an electron of energy E incident on the scattering region on the l transverse mode. On the left contact the solution will be of the form

$$\psi^l_{n,m} = \frac{1}{\sqrt{\mathscr{N}_l}}\,\mathrm{e}^{\mathrm{i}\frac{2\pi l}{M}m}\,\mathrm{e}^{\mathrm{i}k_l a_z n} + \sum_{j=1}^{M}\hat{r}_{lj} \times \frac{1}{\sqrt{\mathscr{N}_j}}\,\mathrm{e}^{\mathrm{i}\frac{2\pi j}{M}m}\,\mathrm{e}^{-\mathrm{i}k_j a_z n}, \quad (m,n)\in \mathrm{I}. \tag{11}$$

On the right contact we have

$$\psi^l_{n,m} = \sum_{j=1}^{M}\hat{t}_{lj}\,\frac{1}{\sqrt{\mathscr{N}_j}}\,\mathrm{e}^{\mathrm{i}\frac{2\pi j}{M}m}\,\mathrm{e}^{\mathrm{i}k_j a_z n}, \quad (m,n)\in \mathrm{III}. \tag{12}$$

The matrices $\hat{r}$ and $\hat{t}$ appearing in these two solutions are the *reflection* and *transmission* matrices and they are responsible for the channel *mixing* due to scattering events. Thus, $\hat{r}_{ij}$ represents the probability amplitude for an electron impinging in channel i to be reflected into the channel j. Similarly $\hat{t}_{ij}$ represents the probability amplitude for an electron impinging in channel i to be transmitted through the scattering region II into the channel j. Note that the solution within region II is unknown. Actually, we are not interested in this solution since all the physics of the scattering problem is contained in the *mixing* matrices $\hat{t}$ and $\hat{r}$. In the following, our main goal will be to relate the elements of $\hat{t}$ and $\hat{r}$ to those of $\mathscr{T}^{(N)}$ in Eq. (6).

We start by re-writing formally Eq. (2) as $\mathscr{H}\psi = E\psi$. Now we perform the following transformation upon the envelope functions:

$$\tilde{\psi} = \hat{t}^{-1}\psi \tag{13}$$

It is easy to see that the Hamiltonian is invariant under such a transformation, that is, $\tilde{\mathscr{H}} \equiv \hat{t}^{-1}\mathscr{H}\hat{t} = \mathscr{H}$. This is clear since $\hat{t}$ and $\mathscr{H}$ formally commute as they act upon different vector spaces. The fact that $\mathscr{H}$ is invariant implies that $\mathscr{T}^{(N)}$ is not affected by transformation (13) so it remains unchanged. In addition, Eqs. (11) and (12) are transformed into

$$\tilde{\psi}^l_{n,m} = \sum_{j=1}^{M}\hat{a}_{lj}\,\frac{1}{\sqrt{\mathscr{N}_j}}\,\mathrm{e}^{\mathrm{i}\frac{2\pi j}{M}m}\,\mathrm{e}^{\mathrm{i}k_j a_z n} + \sum_{j=1}^{M}\hat{b}_{lj} \times \frac{1}{\sqrt{\mathscr{N}_j}}\,\mathrm{e}^{\mathrm{i}\frac{2\pi j}{M}m}\,\mathrm{e}^{-\mathrm{i}k_j a_z n}, \quad (m,n)\in \mathrm{I} \tag{14}$$

and

$$\tilde{\psi}^l_{n,m} = \frac{1}{\sqrt{\mathscr{N}_l}}\mathrm{e}^{\mathrm{i}\frac{2\pi l}{M}m}\,\mathrm{e}^{\mathrm{i}k_l a_z n}, \quad (m,n)\in \mathrm{III}, \tag{15}$$

respectively, where we have defined $\hat{b}_{lj} \equiv \sum_{s=1}^{M}\hat{t}^{-1}_{ls}\hat{r}_{sj}$ and $\hat{a}_{lj} \equiv \hat{t}^{-1}_{lj}$. For each channel l we can write the transform of Eq. (6) as

$$\begin{pmatrix}\tilde{\phi}^l_0\\ \tilde{\phi}^l_1\end{pmatrix} = \mathscr{T}^{(N)}\begin{pmatrix}\tilde{\phi}^l_N\\ \tilde{\phi}^l_{N+1}\end{pmatrix}. \tag{16}$$

Now, introducing the definitions

$$\mathscr{A}^0 \equiv A^0_{jm} = \frac{1}{\sqrt{\mathscr{N}_j}}\,\mathrm{e}^{\mathrm{i}\frac{2\pi j}{M}m},$$

$$\mathscr{B}^0 \equiv \mathscr{A}^0,$$

$$\mathscr{A}^1 \equiv A^1_{jm} = \frac{1}{\sqrt{\mathscr{N}_j}}\,\mathrm{e}^{\mathrm{i}\frac{2\pi j}{M}m}\,\mathrm{e}^{\mathrm{i}k_j a_z},$$

$$\mathscr{B}^1 \equiv B^1_{jm} = \frac{1}{\sqrt{\mathscr{N}_j}}\,\mathrm{e}^{\mathrm{i}\frac{2\pi j}{M}m}\,\mathrm{e}^{-\mathrm{i}k_j a_z},$$

$$\hat{a}^l = \begin{pmatrix}\hat{a}_{l1}\\ \hat{a}_{l2}\\ \vdots\\ \hat{a}_{lM}\end{pmatrix}, \qquad \hat{b}^l = \begin{pmatrix}\hat{b}_{l1}\\ \hat{b}_{l2}\\ \vdots\\ \hat{b}_{lM}\end{pmatrix}, \tag{17}$$

we arrive at the following transformed equation (16) written in terms of the elements of the mixing matrices:

$$\begin{pmatrix}\tilde{\phi}^l_0\\ \tilde{\phi}^l_1\end{pmatrix} = \begin{pmatrix}\mathscr{A}^0 & \mathscr{B}^0\\ \mathscr{A}^1 & \mathscr{B}^1\end{pmatrix}\begin{pmatrix}\hat{a}^l\\ \hat{b}^l\end{pmatrix} = \mathscr{T}^{(N)}\begin{pmatrix}\tilde{\phi}^l_{N-1}\\ \tilde{\phi}^l_N\end{pmatrix}, \tag{18}$$

and, finally, we have

$$\begin{pmatrix} \hat{a}^l \\ \hat{b}^l \end{pmatrix} = \begin{pmatrix} \mathscr{A}^0 & \mathscr{B}^0 \\ \mathscr{A}^1 & \mathscr{B}^1 \end{pmatrix}^{-1} \mathscr{T}^{(N)} \begin{pmatrix} \tilde{\phi}^l_{N-1} \\ \tilde{\phi}^l_N \end{pmatrix}, \qquad (19)$$

that give us the matrix elements $\hat{a}_{lj}$ and $\hat{b}_{lj}$ with $j = 1,2,\ldots,M$ for each channel l in terms of the product of two known matrices and the transformed solutions (15) at the right contact for the l channel. It is worth noticing that all the scattering information is contained in the transfer matrix $\mathscr{T}^{(N)}$. Thus, this quantity turns out to be the fundamental object in the resolution of the scattering problem.

2.4. Conductance and current

Once $\hat{a}$ and $\hat{b}$ have been calculated, obtaining $\hat{t}$ and $\hat{r}$ is an easy task. However, the matrices calculated this way are the *response* matrices that contains some non-physical information. This non-physical information comes from the fact that we have been considering *all* the mathematical solutions of the scattering problem, including those diverging at infinity. These solutions are those for which momentum in Eq. (10) is an imaginary number. In order to avoid the unphysical solutions we will cancel out all the elements on $\hat{t}$ for which the incoming and/or the outgoing transverse quantum number l satisfy the following condition:

$$E < 2t_y \left(\cos \frac{2\pi l}{M} - 1 \right). \qquad (20)$$

Once the physical mixing matrices are known, particularly the transmission matrix $\hat{t}$, we can use them to calculate different physical quantities like the conductance or the electric current. From the Landauer–Büttiker formalism [13], the zero-temperature two-leads multichannel conductance can be calculated using de Fisher–Lee formula [14]

$$G = \frac{2e^2}{h} \mathrm{Tr}(\hat{t}^\dagger \hat{t}). \qquad (21)$$

In order to calculate the electric current due to an applied field F we have to modify slightly our equations and further approximations are needed. First of all, we consider perfect leads, so no voltage drop occurs within the contacts. Besides, we will not consider the contribution to the current of electrons incident from the right contact. This is a good approximation provided $eV > E_\mathrm{F}$, where V is the voltage drop along the region I and E_F is the electron Fermi level on the contacts. Finally, we will assume zero temperature so no carrier statistics will be taken into account.

When an electric field applied along the growth direction is considered, the potential $U(y,z)$ in Eq. (1) has to be replaced by $U(y,z) + U_\mathrm{F}(z)$, where U_F is constant in the contacts ($U_\mathrm{F}(z) = 0$ in region I and $U_\mathrm{F}(z) = -eV$ in region III) and behaves linearly in region II, namely $U_\mathrm{F}(z) = -eFz$. Here F is the applied electric field and $V = FL$ is the voltage drop across the scattering region whose length is L. The electron momentum on the right contact now reads

$$q_l = \frac{1}{a_z} \cos^{-1} \left\{ \frac{1}{2t_z} \left[E + eV - 2t_y \left(\cos \frac{2\pi l}{M} - 1 \right) \right] + 1 \right\}, \quad (m,n) \in \mathrm{III} \qquad (22)$$

and solution in region III changes to

$$\psi^l_{n,m} = \sum_{j=1}^{M} \hat{t}_{lj} \frac{1}{\sqrt{\mathscr{N}_j}} \mathrm{e}^{\mathrm{i}\frac{2\pi j}{M} m} \mathrm{e}^{\mathrm{i}q_j a_z n}. \qquad (23)$$

Bearing in mind all the approximations considered so far, a new transfer matrix $\mathscr{T}^{(N)}$ can be calculated for each value of F. Inserting solution (23) in Eq. (19) we can obtain the mixing matrices for a given applied field and then, using them, calculate the electric current induced by that field. From the expression for the probability current we can write the discretized version of the electronic current density contribution of channel l along the applied field direction across the right lead (calculated on a slide n within the region III) as

$$j^l_z = \mathrm{i} \frac{et_z a_z}{\hbar a_y} \frac{1}{M} \sum_{m=1}^{M} \mathrm{Im}[(\psi^l_{n,m})^* \psi^l_{n+1,m}]. \qquad (24)$$

In order to calculate the total current density across the sample, we just need to sum up over all the allowed transverse states below the Fermi level at the left contact, that is

$$j_z = \mathrm{i} \frac{et_z a_z}{2\pi\hbar a_y} \frac{1}{M} \sum_{m=1}^{M} \sum_{l=1}^{M} \int_0^{k^l_\mathrm{F}} \mathrm{Im}[(\psi^l_{n,m})^* \psi^l_{n+1,m}] \, \mathrm{d}k. \qquad (25)$$

Notice that the electron momentum in the z direction, k, varies continuously as the energy for an incident electron can take values from 0 to E_F. Here, k_F^l is the component of the electron momentum along the z direction for an incident electron with transverse quantum number l and an incident energy E_F. Using the transmission matrix elements we finally arrive at

$$j_z = \mathrm{i}\,\frac{et_z a_z}{2\pi\hbar a_y}\,\frac{1}{M}\sum_{m=1}^{M}\sum_{l=1}^{M}\int_0^{k_F^l}\sum_{j=1}^{M}\sum_{s=1}^{M}\hat{t}_{lj}^{*}\hat{t}_{ls}\,\frac{1}{\sqrt{\mathcal{N}_s\mathcal{N}_j}} \times \mathrm{e}^{\mathrm{i}\frac{2\pi(s-j)m}{M}}\,\mathrm{e}^{\mathrm{i}(q_s-q_j)a_z n}[\mathrm{e}^{\mathrm{i}q_s a_z}-\mathrm{e}^{-\mathrm{i}q_j a_z}]\,\mathrm{d}k. \quad (26)$$

The results we have obtained so far provide an exact, although nonclosed, analytical description of *any* two-dimensional heterostructure based on wide-gap semiconductors, whenever the Ben Daniel–Duke equation holds valid. Let us stress that the generalization to three-dimensional heterostructures is fairly straightforward. With these results at hand, we can compute the transport magnitudes we mentioned above. All expressions are very simple and suitable for an efficient numerical treatment for any specific case. We will now evaluate them for unintentionally disordered DBS to describe the relevant features of the model.

3. Models of disorder

Unintentional disorder appearing during growth in *actual* heterostructures depends critically on the growth conditions. There exist several techniques, like scanning tunneling microscopy [15–17] and X-ray scattering [18], which have been applied in recent years to quantitatively determine structural properties of multilayers and superlattices. Precise information about the nature and extent of defects at interfaces is now available. Following Mäder et al., disorder in heterostructures can be classified into two categories, namely lateral and vertical [19]. Lateral disorder occurs whenever one semiconductor protrudes into the other, forming chemically mixed interfaces, steps and islands. As a consequence, the interface is not flat and translational symmetry in the plane perpendicular to the growth direction is broken. On the other side, vertical disorder is observed whenever layer thicknesses fluctuate around their nominal values. Compositional disorder due to different local Al concentration in each $Ga_{1-x}Al_xAs$ layer can be viewed as mixing of vertical and lateral disorder.

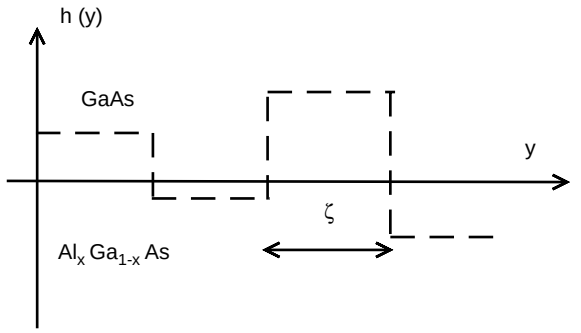

Fig. 2. Steps and islands modeling lateral disorder (roughness) at the interface between two epilayers.

3.1. Lateral disorder

In order to treat lateral disorder we have considered the formation of islands on the interface between two consecutive layers, all of them having identical lateral sizes, and being consecutive to each other. In our model islands have heights that are randomly distributed (see Fig. 2). It is possible to express the rough profile of the interface between two consecutive layers defining the following height function:

$$h(y) = \eta\sum_n w_n\{\Theta(y-n\zeta) + \Theta[(n+1)\zeta - y] - 1\}. \quad (27)$$

Here $h(y)$ represents the deviation from the flat surface at position y, Θ is the Heavyside theta function, ζ is the island width, w_n is a random variable associated to the nth island that controls the fluctuation around the mean value, and η is the largest deviation—in absolute value—assuming that the w_n's are uniformly distributed between -1 and 1. Hereafter η will be referred to as degree of *lateral disorder*. In the following, two models will be introduced. First of all, uncorrelated disorder will be considered, for which the random variables w_n take values from -1 to 1 uniformly, satisfying the following correlator $\langle w_n w_m\rangle = \delta_{nm}/3$, where δ_{nm} is the Kronecker delta. This kind of correlator implies that the surface height at each point of the growing surface is independent

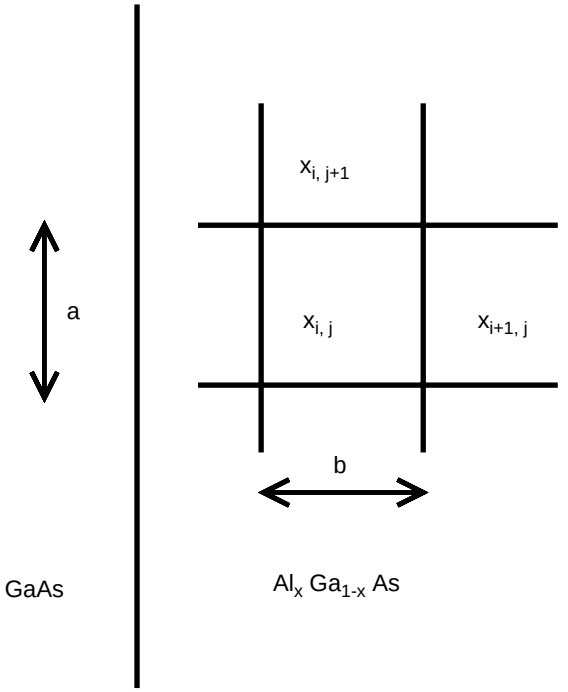

Fig. 3. Schematic view of the Al fraction mesh in the barrier showing the distribution of Al concentration at different sites.

of the height on every point over the rest of the interface. However, experimental data and theoretical models of molecular-beam-epitaxy growth processes [20] indicate that the heights of the surface at distant points are strongly correlated. To mimic this situation, we will consider a second model of lateral disorder where the w_n's are normally distributed with zero mean satisfying the exponential correlator $\langle w_n w_m \rangle = \exp(-|n-m|/\xi)/3$, where ξ is the correlation length of the disorder.

3.2. Compositional disorder

Compositional disorder in GaAs–$Al_xGa_{1-x}As$ heterostructures is due to the lack of spatial uniformity of the Al mole fraction during the heterostructure growth process. We will simulate compositional disorder by defining a spatial two-dimensional mesh over the $Al_xGa_{1-x}As$ barriers, as shown in Fig. 3. We will associate a value x_{ij} for the Al mole fraction to each region of the mesh. This value will fluctuate randomly around the nominal value of the Al fraction on the barrier $\bar{x}$. Thus we can write

$$x_{ij} = \bar{x} + \Omega w_{ij}, \tag{28}$$

where Ω is the maximum fluctuation of the Al mole fraction, and w_{ij} is a random variable related to the (i,j) point of the mesh, taking values uniformly between -1 and 1. Note that the overall averaged mole fraction is equal to $\bar{x}$.

4. Results

We have performed several numerical calculations in order to study the effect of both lateral and compositional disorder over the transport properties of DBS made of GaAs–$Al_xGa_{1-x}As$ heterostructures. All the calculations correspond to zero-temperature conditions unless others are stated.

4.1. Uncorrelated lateral disorder

We start by considering the effect of the interface roughness, characterized by the degree of lateral disorder η given in Eq. (27), on the conductance. Fig. 4 shows the conductance calculated for different values of η. Here $a_y = 10$ nm, $a_z = 0.3$ nm, $\zeta = 20$ nm, $M = 50$, and $N = 38$. The barrier widths are 2.1 nm. Their heights are also the same, 0.3 eV, and the well width is 4.8 nm. The curves correspond to an ensemble average of the conductance curves over 100 different realizations of the lateral disorder. Three different values of η were studied, namely $\eta = 0$ (perfect DBS), $\eta = 0.3$ nm (largest fluctuation of the order of one monolayer) and $\eta = 0.6$ nm (largest fluctuation of the order of two monolayers). As a main result, it can be seen in Fig. 4 that increasing the degree of lateral disorder, η, results in a decrease of the conductance at the resonant energy. In order to check the effects of temperature on the conductance we have plotted this quantity at two different values of the temperature, $T = 77$ and 300 K, using the Engquist–Anderson formula [21]. Fig. 5 shows the conductance for an ordered system and a disordered one with $\eta = 0.3$ nm. In both the cases it can be observed that the conductance peak widens as temperature is increased and its height is reduced. A reduction of the conductance is still observed as a consequence of lateral disorder.

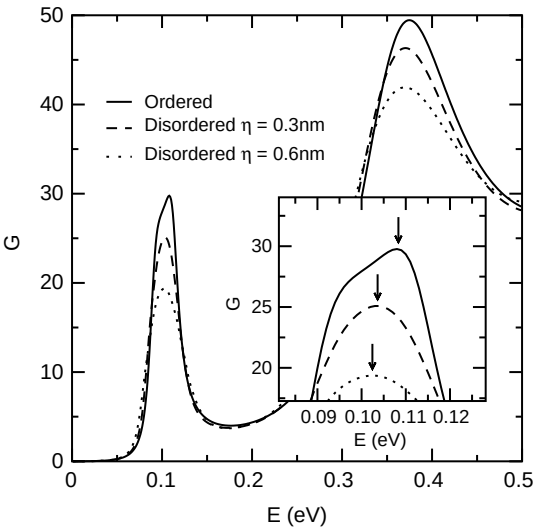

Fig. 4. Conductance in units of $2e^2/h$ of an ordered DBS compared with that of a disordered DBS for two different values of the degree of lateral disorder η. The disordered results were obtained by averaging over 100 realizations of the disorder. The inset shows the shift of the first resonant peak towards lower energy on increasing the degree of disorder.

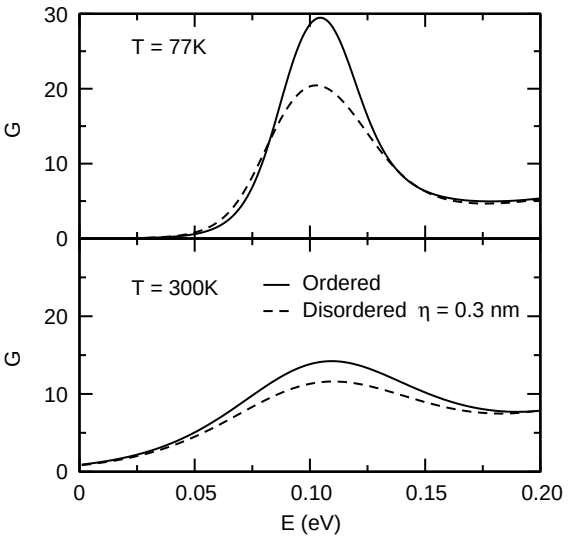

Fig. 5. Conductance in units of $2e^2/h$ of an ordered DBS compared with that of a disordered DBS for two different values of the temperature, $T = 77$ and 300 K. The disordered results were obtained by averaging over 100 realizations of the disorder. $\eta = 0.3$ nm in the disordered case.

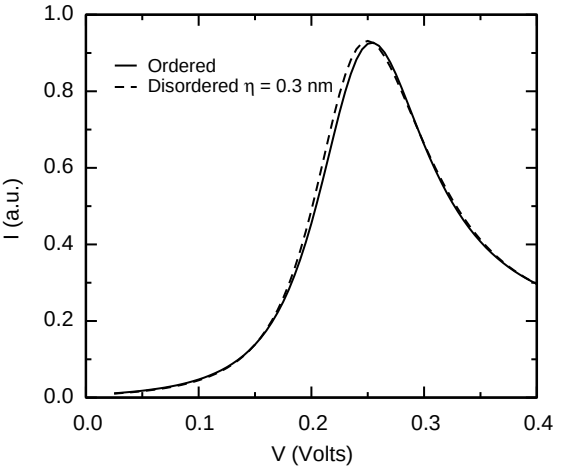

Fig. 6. Current in arbitrary units as a function of the applied bias along the z direction for an ordered DBS and a disordered one. Curve was calculated by averaging over 50 realizations of the disorder.

Notice that the zero-temperature resonant conductance peak slightly widens due to the fluctuations of its energy for each realization of the disorder. Besides, an additional effect can be seen, that is, as the degree of lateral disorder η increases the conductance peak shifts to smaller energies. This effect will be important later in order to explain the j–V characteristic. Regarding the effect of the size of the islands, ζ, we have observed that it can be neglected unless this size is of the order of the electron wavelength, that is, for $\zeta \gg \lambda_e$ the conductance does not depend on ζ. As expected, when $\zeta \sim \lambda_e$ the electron starts to *see* the disorder and then the conductance increases as ζ decreases, as shown in Fig. 7. For energies about 0.1 eV this transition takes place at sizes $\zeta \sim 10$ nm [12].

Current as a function of the applied bias is depicted in Fig. 6. For this calculation we have chosen $a_y = 10$ nm, $a_z = 0.1$ nm, $\zeta = 10$ nm, $M = 20$ and $N = 77$. The barrier widths are 2.1 nm for both the emitter and the collector and their heights are also the same, 0.25 eV. The well width is 2.9 nm. Curves shown in Fig. 6 correspond to an average over 50 different realizations of the lateral disorder. The Fermi level was fixed at 20 meV, the maximum applied bias was 0.5 V, and η=0.3 nm. Surprisingly, current in disordered DBS is larger than that calculated in ordered DBS. This counterintuitive result can be explained

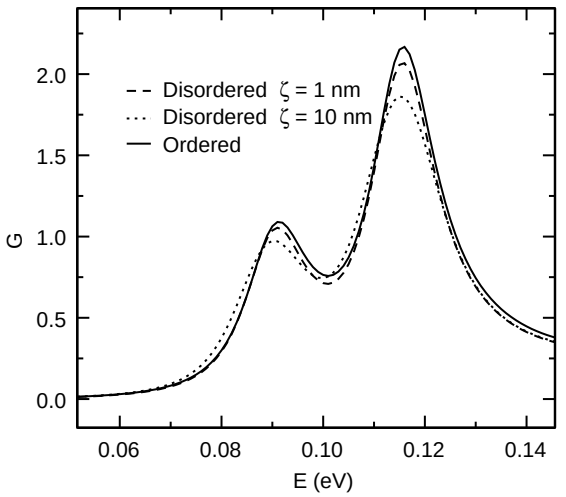

Fig. 7. Conductance in units of $2e^2/h$ as a function of the size of the islands for $\zeta \sim \lambda_e$ (dotted line) and $\zeta < \lambda_e$ (dashed line). Curves were calculated by averaging over 50 realizations of the disorder.

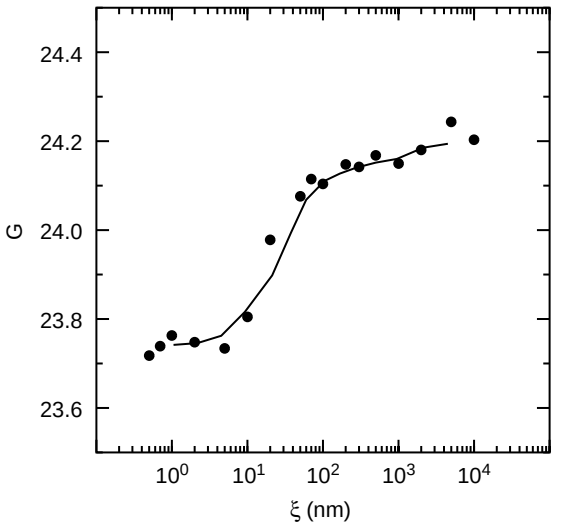

Fig. 8. Conductance in units of $2e^2/h$ of a disordered DBS where disorder is exponentially correlated, as a function of the correlation length, for a fixed energy $E_c = 102.5$ meV. Each point of the curve was calculated by averaging over 50 realizations of the correlated disorder with fixed correlation length ξ.

recalling that conductance peak shifted to lower energies, as mentioned above. The lowering of the conductance peak can be understood assuming that surface roughness makes the effective width of the quantum well larger than its nominal value. This would imply a lower transmission resonance so that the current peak shifts toward lower bias. But an effective wider well implies a higher current too, so in some statistical sense the current for the disordered DBS will be higher.

4.2. Correlated lateral disorder

Upto now we have been considering only lateral uncorrelated roughness at the heterojunctions. We have also calculated the conductance for a DBS in which interface roughness is an exponentially correlated random variable, as described previously. Fig. 8 shows the conductance at a given energy about the conductance resonance for the ordered case (where fluctuations are lower), $E_c = 0.1025$ eV, when the correlation length varies several orders of magnitude. Physical parameters of the DBS are the same as in Fig. 4. The size of the islands is 20 nm and the degree of lateral disorder is $\eta = 0.3$ nm. An average over 50 realizations of the disorder has been performed. It can be observed that the conductance increases as the correlation length increases. Two asymptotic regimes are clearly observed for small and large correlation lengths, respectively. The former limit, $\xi \to 0$, can be understood as the situation previously studied where lateral disorder is uncorrelated. From a close inspection of Fig. 8 we come to the remarkable result that this uncorrelated limit correctly describes transport properties whenever the correlation length does not exceed 10 nm. Then we are lead to an important conclusion, namely those models of electron transport in disordered DBS based on the assumption that disorder is uncorrelated would yield right values of the conductance even if the correlation length is not vanishing but fairly large. There is no need to mention that uncorrelated disordered models are much more convenient for analytical work than correlated ones. The size of the plateau for which correlations in the disorder do not play an essential role is governed by the size of the islands, ζ, as might be expected. This is due to the fact that only correlations of the lateral disorder whose correlation length is greater than the size of the islands affect electron motion. For these sizes, the conductance increases as the correlation length

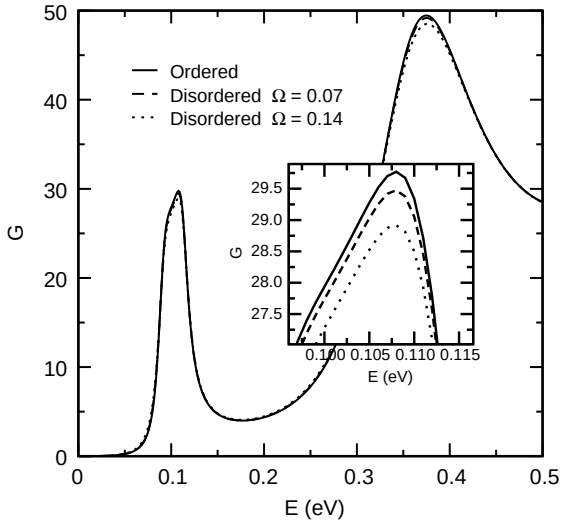

Fig. 9. Conductance in units of $2e^2/h$ for an ordered DBS compared with that of a DBS with only compositional disorder for two different values of Ω. The inset shows enlarged view of the first resonant peak.

becomes larger. This trend is observed up to sizes of the order of 100 nm, namely the system size in the y direction, and then the second regime appears. In this regime the limiting value of the conductance can be calculated as an average over different ordered DBS, each one having barrier widths distributed normally.

4.3. Compositional disorder

Having discussed the effects of interface roughness, let us now present our results regarding compositional disorder. To clarify the effects of local fluctuations of the Al mole fraction, we assume that the interfaces are perfectly flat and that the width of the different semiconductor layers are exactly their nominal values, i.e., we neglect fluctuations of their widths. We show typical results in Fig. 9, where physical parameters are the same as in Fig. 4. The spatial extent of the region where the Al mole fraction can be assumed locally constant was taken to be $a = 10$ nm and $b = 1$ nm (see Fig. 3). It can be observed that, for fluctuations as large as $\Omega = 0.14$, that is, height fluctuations of about 0.1 eV, when averaging over 100 realizations the conductance is almost unchanged (only 3% variation). This behavior is a consequence of the small electron probability amplitudes within the barriers, where compositional disorder is considered to appear. In other words, even moderately high spatial inhomogeneities in the barriers scarcely affect the electron envelope function. Thus, we can conclude that the effects of compositional disorder can be disregarded as they are much smaller than those of lateral disorder.

5. Conclusions

In this paper we have presented a method to study vertical transport in two-dimensional semiconductor heterostructures including some aspects present in real samples, i.e., growth imperfections and current leads. In particular we have focused on the effects of unintentional disorder on electron transport when translational symmetry along the normal plane to the growth direction is broken by structural imperfections. Two different kinds of disorder leading to electron scattering have been presented, namely lateral disorder and compositional disorder. Lateral disorder appears as a consequence of the roughness present at the interface between GaAs and $Al_xGa_{1-x}As$. Compositional disorder is due to the inhomogeneity of the Al mole fraction occurring during the growth process of $Al_xGa_{1-x}As$ epilayers. We have shown that the main effect of the lateral disorder is to decrease the DBS conductance. When correlations are introduced, conductance starts improving, the larger the correlation length the higher the conductance. However, current shows a surprising behavior, as it is higher in the disordered case than in the ordered one. We attributed it to an energy shift of the transmission resonance of the DBS. Another important conclusion regards the validity of uncorrelated disordered models; they provide right values of the conductance whenever the actual correlation length does not exceed the system size, thus allowing a simpler theoretical description. Finally, we have shown that the effect of compositional disorder can be disregarded as it is much smaller than the effect of lateral disorder. The present model provides a quantitative picture of the effects of lateral disorder on the conductance. It should be noticed that the peak-to-valley ratios are larger than that obtained in experiments [22]. Therefore, our results are the starting point for further developments, including electron–electron and electron–phonon coupling.

This improved model could be directly compared with actual experiments.

Acknowledgements

The authors want to thank V.A. Malyshev for the critical reading of the manuscript. Work in Madrid was supported by DGI-MCyT (Project MAT2000-0734) and CAM (Project 07N/0075/2001). P. Orellana would like to thank Milenio ICM P99-135-F and Cátedra Presidencial de Ciencias for financial support.

References

[1] T.C.L.G. Sollner, W.D. Goodhue, P.E. Tannenwald, C.D. Parker, D.D. Peck, Appl. Phys. Lett. 43 (1984) 588.
[2] B. Ricco, M.Ya. Azbel, Phys. Rev. B 29 (1984) 1970.
[3] N.S. Wingreen, K.W. Jacobsen, J.W. Wilkins, Phys. Rev. Lett. 61 (1988) 1396.
[4] W. Cai, T.F. Zheng, P.H. Hu, B. Yudanin, M. Lax, Phys. Rev. Lett. 63 (1989) 418.
[5] V.A. Chitta, C. Kutter, R.E.M. de Bekker, J.C. Maan, S.J. Hawksworth, J.M. Chamberlain, M. Henini, G. Hill, J. Phys.: Condens. Matter 6 (1994) 3945.
[6] J. Iñarrea, G. Platero, C. Tejedor, Semicond. Sci. Technol. 9 (1994) 515.
[7] A. Levy Yeyati, F. Flores, E.V. Anda, Phys. Rev. B 47 (1993) 10 543.
[8] P. Orellana, F. Claro, Appl. Phys. Lett. 75 (1999) 1643.
[9] P. Orellana, F. Claro, E. Anda, Phys. Rev. B 62 (2000) 9959.
[10] U. Penner, H. Rücker, I.N. Yassievich, Semicond. Sci. Technol. 13 (1998) 709.
[11] V.D. Freilikher, S.A. Gradeskul, Prog. Opt. 30 (1991) 137.
[12] L.E. Henrickson, K. Hirakawa, J. Frey, T. Ikoma, J. Appl. Phys. 71 (1992) 3883.
[13] R. Landauer, IBM J. Res. Dev. 1 (1957) 223;
M. Büttiker, Phys. Rev. Lett. 57 (1986) 1761;
M. Büttiker, IBM J. Res. Dev. 32 (1988) 63;
M. Büttiker, IBM J. Res. Dev. 32 (1988) 317.
[14] D. Fisher, P.A. Lee, Phys. Rev. B 23 (1981) 6851.
[15] R.M. Feenstra, D.A. Collins, D.Z.-Y. Ting, M.W. Wang, T.C. McGill, Phys. Rev. Lett. 72 (1994) 2749.
[16] H.W. Salemik, O. Albrektsen, P. Koenraad, Phys. Rev. B 45 (1992) 6946.
[17] S. Gwo, K.-J. Chao, C.K. Shih, K. Sandra, B.G. Streetman, Phys. Rev. Lett. 71 (1993) 1883.
[18] M. Jergel, V. Holý, E. Majková, Š. Luby, R. Senderák, H.J. Stock, D. Menke, U. Kleineberg, U. Heinzmann, Physica B 253 (1998) 28.
[19] K.A. Mäder, L.-W. Wang, A. Zunger, J. Appl. Phys. 78 (1995) 6639.
[20] A.L. Barabási, H.E. Stanley, Fractal Concepts in Surface Growth, Cambridge University Press, Cambridge, 1995.
[21] H.L. Engquist, P.W. Anderson, Phys. Rev. B 24 (1981) 1151.
[22] J.H. Davies, The Physics of Low-Dimensional Semiconductors, Cambridge University Press, Cambridge, 1998.